

Microstructure and creep properties of Mg-4Al-2Sn-1(Ca,Sr) alloys

B. H. KIM, K. C. PARK, Y. H. PARK, I. M. PARK

Department of Material Science and Engineering, Pusan National University,
San 30 Jangjeon-dong, Geumjeong-gu, Busan 609-735, Korea

Received 23 September 2009; accepted 30 January 2010

Abstract: The effects of Ca and Sr addition on the microstructure and creep properties of Mg-4Al-2Sn alloys were examined. Tensile tests at 25 °C and 200 °C and creep tests at 150 °C and 200 °C were carried out to estimate the room temperature and high temperature mechanical properties of these alloys. The microstructure of the Mg-4Al-2Sn alloy showed dendritic α -Mg, Mg₁₇Al₁₂ and Mg₂Sn phases. The latter two phases precipitated along the grain boundaries. The addition of Ca and Sr resulted in the formation of ternary CaMgSn and SrMgSn phases within the grain. The grain size was reduced slightly with the addition of Sr and Ca. The tensile strength was decreased by the addition of Ca and Sr at room temperature. However, the high temperature tensile strength was increased. The creep strength was improved by the addition of Ca and Sr.

Key words: magnesium alloys; Ca; Sr; void initiation; mechanical properties; creep mechanism

1 Introduction

Magnesium alloys have great potential for high performance structural applications owing to their high specific strength, low density, excellent machineability and good damping characteristic. These alloys are used in the automotive and aerospace industries to improve fuel efficiency by reducing the vehicle weight[1–3]. Commercial Mg-Al alloys, such as AZ91 and AM60 alloys, are currently used in automotive components, such as cylinder heads, airbag housings, steering wheels and seat flames. However, the service temperatures of these Mg-Al alloys are limited to 150 °C due to the low creep properties[4]. In order to broaden the application fields of Mg-Al alloys, it is essential to improve the creep strength. The most common way of improving the elevated temperature properties is through the formation of thermally stable precipitates or dispersoids along the grain boundaries to resist the deformation caused by grain boundary sliding[5]. Rare earth elements are the most effective alloying elements for such purposes which result in significant improvement in the elevated temperature properties[6]. However, the high cost of these alloys compared with conventional magnesium alloys has limited their applications. Sn, Ca and Sr are relatively inexpensive alloying elements. Sn can increase

the strength through solution strengthening. In addition, the solubility of Sn in α -Mg decreases sharply with decreasing the temperature, which can further improve the mechanical properties through aging[7]. The addition of Ca and Sr to Mg-Al alloys can refine the as-cast microstructure of the alloys[8–10] and improve the mechanical properties at room or high temperatures[11–12]. However, there are few reports on the effects of Ca and Sr addition on the creep properties of Mg alloys. In this study, the microstructural stability of Mg-4Al-2Sn-1(Ca, Sr) alloys was examined. Creep tests were performed to estimate the high temperature mechanical properties.

2 Experimental

Pure magnesium (99.8%), aluminum (99.8%), tin (99.8), and Mg-40%Ca and Mg-40%Sr (mass fraction) master alloys were used in this study. The alloys were melted at 750 °C in a mild steel crucible under CO₂+SF₆ atmosphere. The molten metal was squeeze cast at 50 MPa for 60 s. Table 1 lists the designations and nominal compositions of the alloys. Microstructural analysis was carried out using an optical microscope and a scanning electron microscope equipped with an energy dispersive X-ray spectrometer. A solution of 3% (volume fraction) Nital was used to etch the samples. The phases were

Table 1 Materials designations and chemical compositions of AT42 system alloys (mass fraction, %)

Alloy	Al	Sn	Ca	Sr	Cu	Fe	Ni	Mg
AT42	4.1	1.9	–	–	0.003	0.004	0.001	Bal.
ATX421	3.9	2.1	1.2	–	0.002	0.005	0.001	Bal.
ATJ421	4.2	1.8	–	1.3	0.002	0.004	0.001	Bal.

analyzed by X-ray diffractometry (XRD) using monochromatic Cu K_{α} radiation in the as-cast state. The dimension of the tensile and creep test specimens was 3 mm×6 mm×30 mm in size.

The tensile tests were carried out at an initial engineering strain rate of 2 mm/min at room temperature and 200 °C. The creep tests were carried out using a lever arm type creep tester where the box chamber (450 mm×250 mm×250 mm) for temperature control was attached. The creep test temperature was 150 °C and 200 °C, and the stress was 50, 60 and 80 MPa. The fractured surface of the creep specimen was observed.

3 Results and discussion

3.1 Microstructure

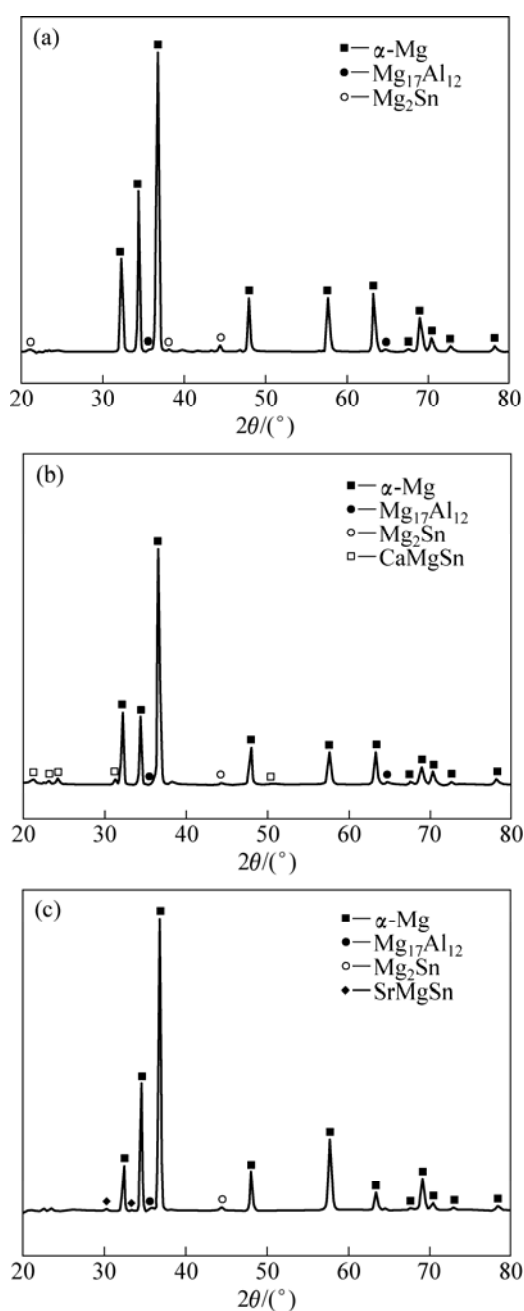
Fig.1 shows XRD patterns of the as-cast alloys. The microstructure of the AT42 alloy (Fig.1(a)) consisted mainly of α -Mg, β - $Mg_{17}Al_{12}$ and Mg_2Sn phases. Ternary $SrMgSn$ and $CaMgSn$ phases were detected with the addition of Ca and Sr. It was assumed that the addition of Ca and Sr to the AT42 alloy suppressed the immediate production of Mg_2Sn , resulting in the formation of ternary phases, such as $CaMgSn$ and $SrMgSn$.

Figs.2 and 3 show the optical microscopy and SEM images of the as-cast alloys. Fig.2 indicated that the as-cast alloys were composed of a primary dendritic α -Mg matrix with non-equilibrium secondary phases. $Mg_{17}Al_{12}$ and Mg_2Sn were formed mainly along the grain boundaries, whereas $CaMgSn$ and $SrMgSn$ were formed within the grain. The grain size was decreased from 85.0 μm to 73.8 μm by the addition of Ca and Sr. SEM-EDS and XRD identified that the feather-like and needle-like phases were $CaMgSn$ and $SrMgSn$, respectively.

3.2 Mechanical properties

Fig.4 shows the stress—strain curves of the alloys at room temperature and 200 °C, and Table 2 lists the mechanical properties of the alloys. The ultimate tensile strength, yield strength and elongation of the AT42 alloy were 161 MPa, 75 MPa and 7.2 %, respectively. However, the ultimate tensile strength and elongation were decreased slightly by the addition of Ca or Sr at room temperature. At elevated temperatures, the ultimate tensile strength, yield strength and elongation of the AT42 alloy were 99 MPa, 60 MPa and 18.5%, respectively. In contrast to the room temperature sample,

the ultimate tensile strength, yield strength and elongation of the ATJ421 alloy were increased to 117 MPa, 73 MPa and 19.2%, respectively. When the mechanical properties were compared between AT42 and ATJ421, room temperature properties were higher in AT42 than ATJ421 while ATJ421 showed better high temperature properties than AT42. Fig.5 shows the non-etched and etched transverse section of a tensile specimen of AT42 containing Ca and Sr at room temperature and 200 °C. Figs.5(a) and (b) respectively show that $CaMgSn$ and $SrMgSn$ phases acted as crack initiation sites during tensile deformation at room temperature. Therefore, it could have a negative effect on

**Fig.1** XRD patterns of AT42 system alloy: (a) AT42; (b) ATX421; (c) ATJ421

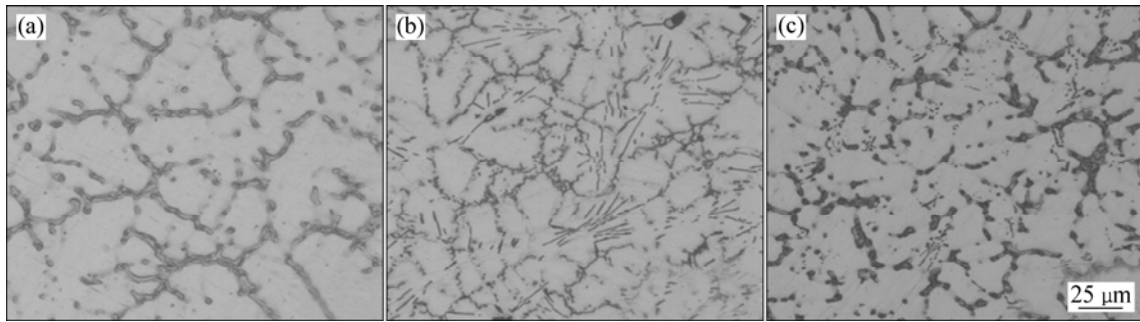


Fig.2 OM images of AT42 alloys: (a) AT42; (b) ATX421; (c) ATJ421

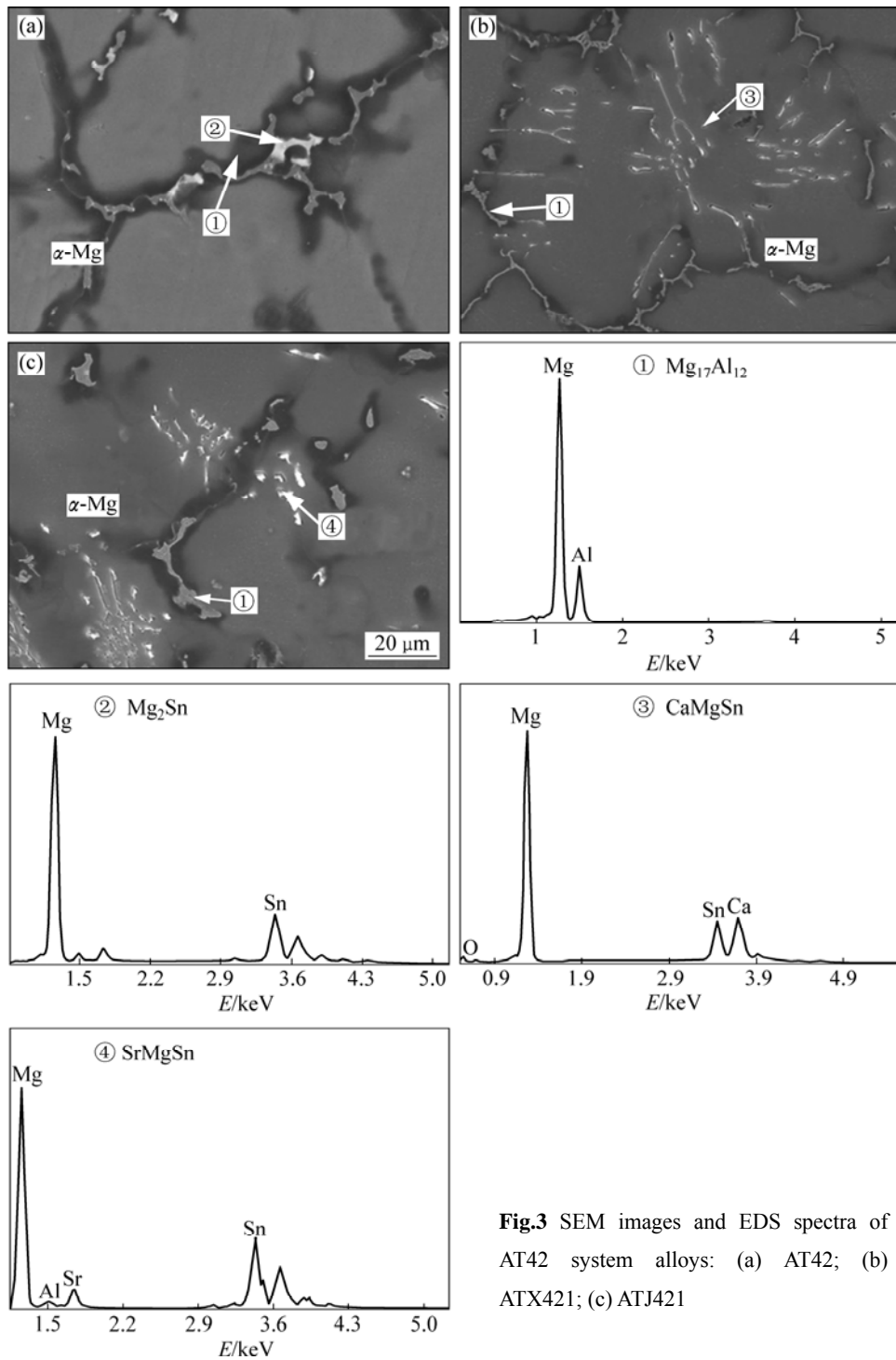


Fig.3 SEM images and EDS spectra of AT42 system alloys: (a) AT42; (b) ATX421; (c) ATJ421

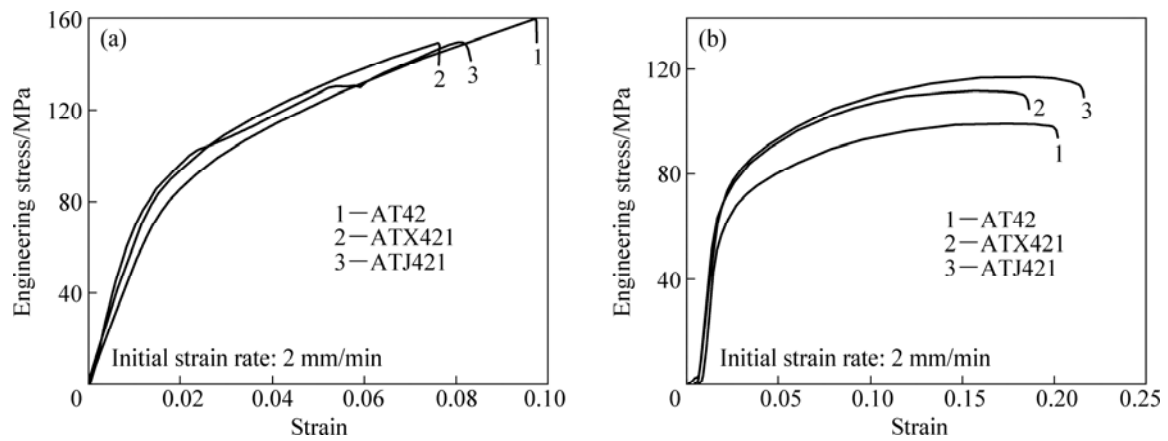


Fig.4 Tensile curves of AT42 system alloys at room temperature (a) and 200 °C (b)

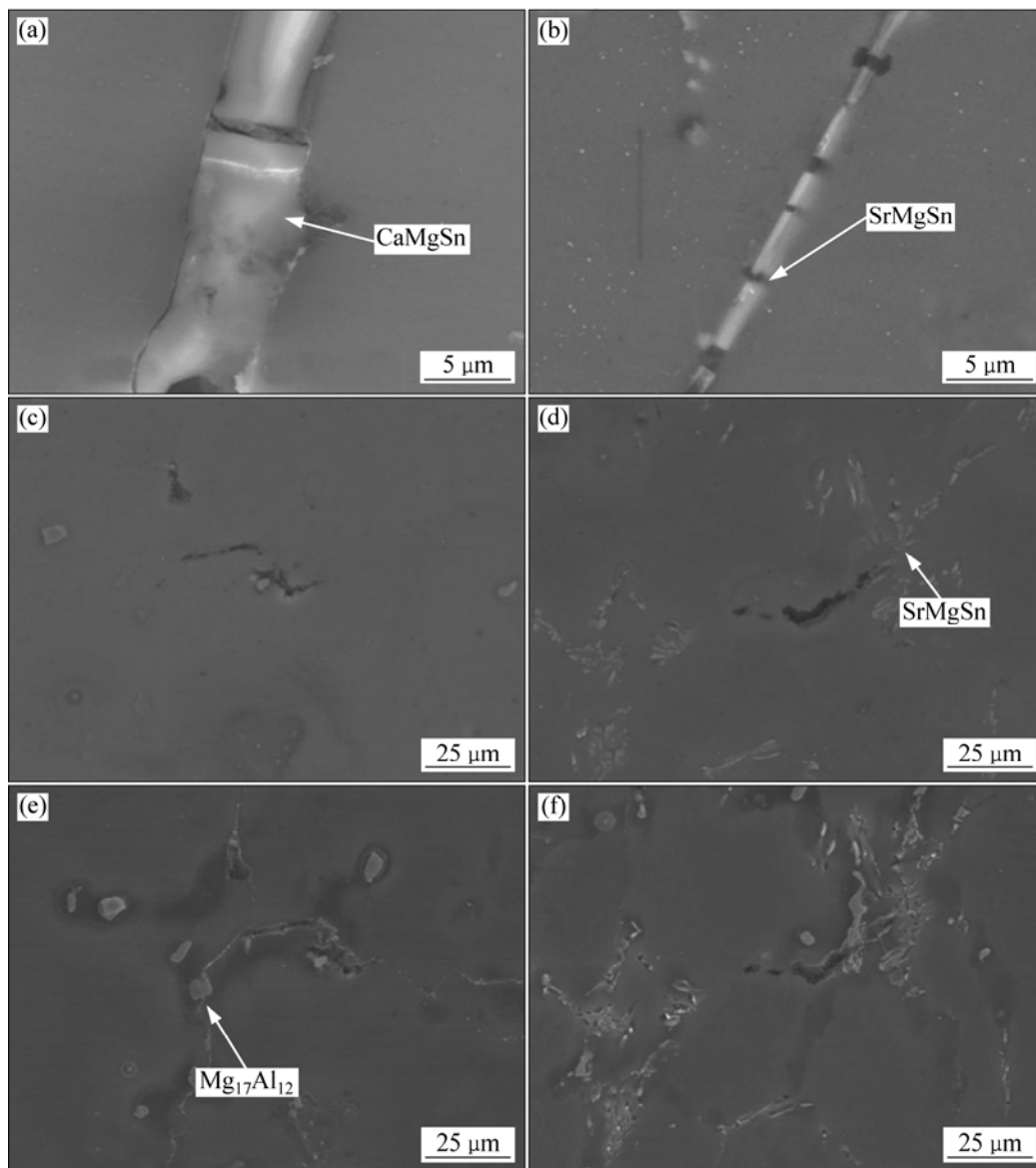


Fig.5 Transverse section of tensile specimen of AT42 system alloys at room temperature: (a) Non-etched ATX421; (b) Non-etched ATJ421, 200 °C; (c) Non-etched AT42; (d) Non-etched ATJ421; (e) Etched AT42; (f) Etched ATJ421

Table 2 Mechanical properties of AT42 system alloys at room temperature and 200

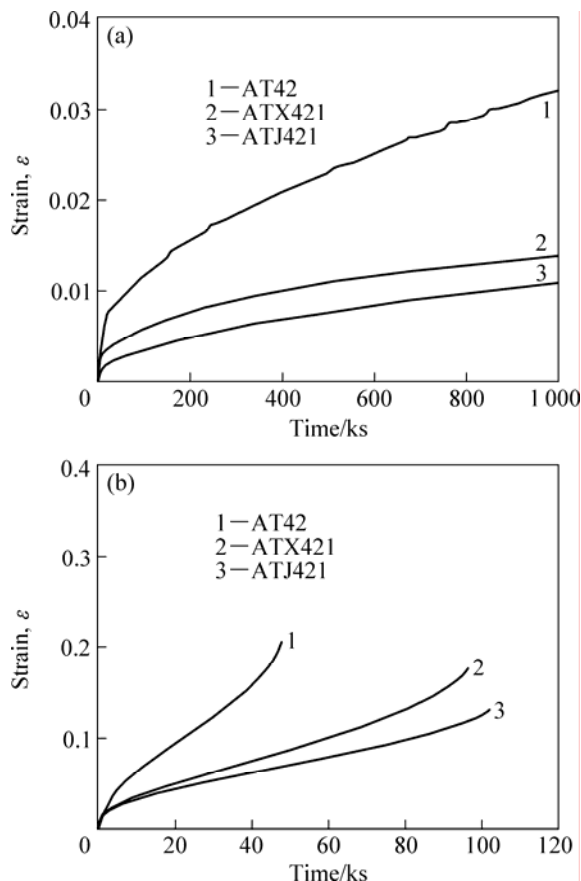
Alloy	Temperature/	σ_b /MPa	$\sigma_{0.2}$ /MPa	δ /%
AT42	RT	75.2	161.1	7.2
	200	60.1	99.2	18.5
ATX421	RTe	85.4	150.0	6.1
	200	72.2	111.6	17.4
ATJ421	RT	86.1	150.2	6.4
	200	73.1	117.3	19.2

RT—Room temperature.

the room temperature tensile properties. At elevated temperatures, the crack was propagated along the grain boundaries and the SrMgSn and CaMgSn phases impeded the crack propagation at grain boundaries, as shown in Figs.5(c)–(f). This means that these phases could positively affect the elevated temperature tensile properties.

3.3 Creep properties

Fig.6 shows the creep strains of the AT42 alloys as a function of time. Under the identical test conditions, the minimum creep rate had the following sequence: AT42>ATX421>ATJ421. At 150 °C and 200 °C with an applied stress of 70 MPa, the addition of Ca and Sr resulted in a lower minimum creep rate compared with

**Fig.6** Creep strains of AT42 system alloys as function of time: (a) 150 °C, 50 MPa; (b) 200 °C, 70 MPa

the AT42 alloy. The stress exponent (n) and activation energy (Q) were calculated to better understand the detailed creep mechanism for alloys. The steady-state creep rate ($\dot{\epsilon}$) can be explained by the following power-law relationship[13]:

$$\dot{\epsilon} = A \frac{D_0 G b}{k T} \left(\frac{\sigma}{G} \right)^n \exp\left(-\frac{Q}{RT}\right) \quad (1)$$

where G is the shear modulus, k is the Boltzmann's constant, b is the length of the Burgers vector, D_0 is the frequency factor, σ is the applied stress and R is the gas constant. Both n and Q can be determined from the creep data collected at various temperatures and stresses, and may be used together to identify the dominant creep mechanism of a material. The stress exponent, n , can be calculated by plotting the logarithm of the minimum creep rate $\dot{\epsilon}$ as a function of the applied stress σ . The activation energy was estimated from the slope of a plot of $\lg \dot{\epsilon}$ as a function of $1/T$.

Table 3 shows the values of the stress exponent and activation energy for these alloys. The stress exponent and activation energy of the AT42 alloy were calculated to be 4.2 and 116 kJ/mol, respectively. These values indicate the dominant creep mechanisms for the alloy under the present test conditions. The stress exponent $n=4-6$ is for dislocation climb controlled creep[14]. The activation energy, $Q=116$ kJ/mol, was higher than the activation energy for grain boundary diffusion (92 kJ/mol) or cross slip (100 kJ/mol) normally observed for the Mg alloys deformed by grain boundary sliding. However, it was lower than the activation energy for the lattice self-diffusion of Mg (135 kJ/mol) observed for Mg alloys deformed by dislocation climb. Table 3 shows that AT42 alloys containing Ca and Sr have larger activation energies than the AT42 alloy. The values of both parameters fit the values for dislocation climb controlled creep, suggesting that the creep of AT42 alloys containing Ca and Sr occurs through dislocation climb controlled creep. The thermally stable Mg₂Sn, CaMgSn and SrMgSn phases pin the grain boundaries and hinder both grain boundary migration and sliding during high temperature deformation.

Fig.7 shows the optical images of the alloys during the creep test at 200 °C, 70 MPa and 48 h. The thermally unstable Mg₁₇Al₁₂ phases coarsened due to the concentration of the stress and constant elevated

Table 3 Values of stress exponent (n) and activation energy (Q) for creep of AT42 system alloys

Alloy	n	Q /(kJ·mol ⁻¹)
AT42	4.2	116
ATX421	5.6	134
ATJ421	5.5	135

temperature. In particular, the microstructure of the AT42 alloy showed significant changes compared with the other alloys. However, AT42 containing the CaMgSn and SrMgSn phases showed little change, and could be considered thermally stable phases compared with $Mg_{17}Al_{12}$. Figs.8 and 9 show the non-etched and etched SEM images of the AT42 system alloys during the creep test. Voids were initiated mainly at $Mg_{17}Al_{12}$ and

propagated along the grain boundaries. On the other hand, the CaMgSn and SrMgSn phases impeded crack propagation, as shown in Fig.10. This suggests that a ternary phase, such as SrMgSn and CaMgSn, has a larger effect on the creep properties than on the room temperature tensile properties. This is because, in the tensile test, the crack is initiated at SrMgSn and CaMgSn, and the fracture strength is decreased significantly.

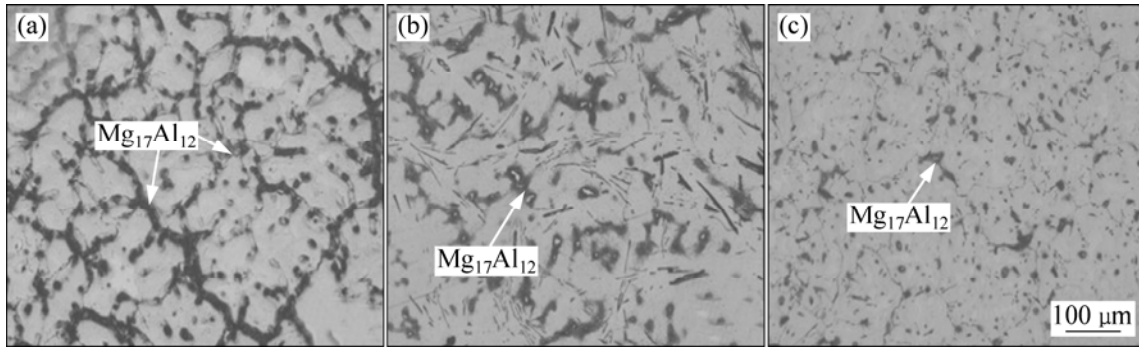


Fig.7 OM images of alloys during creep test at 200 °C, 70 MPa and 48 h: (a) AT42; (b) ATX421; (c) ATJ421

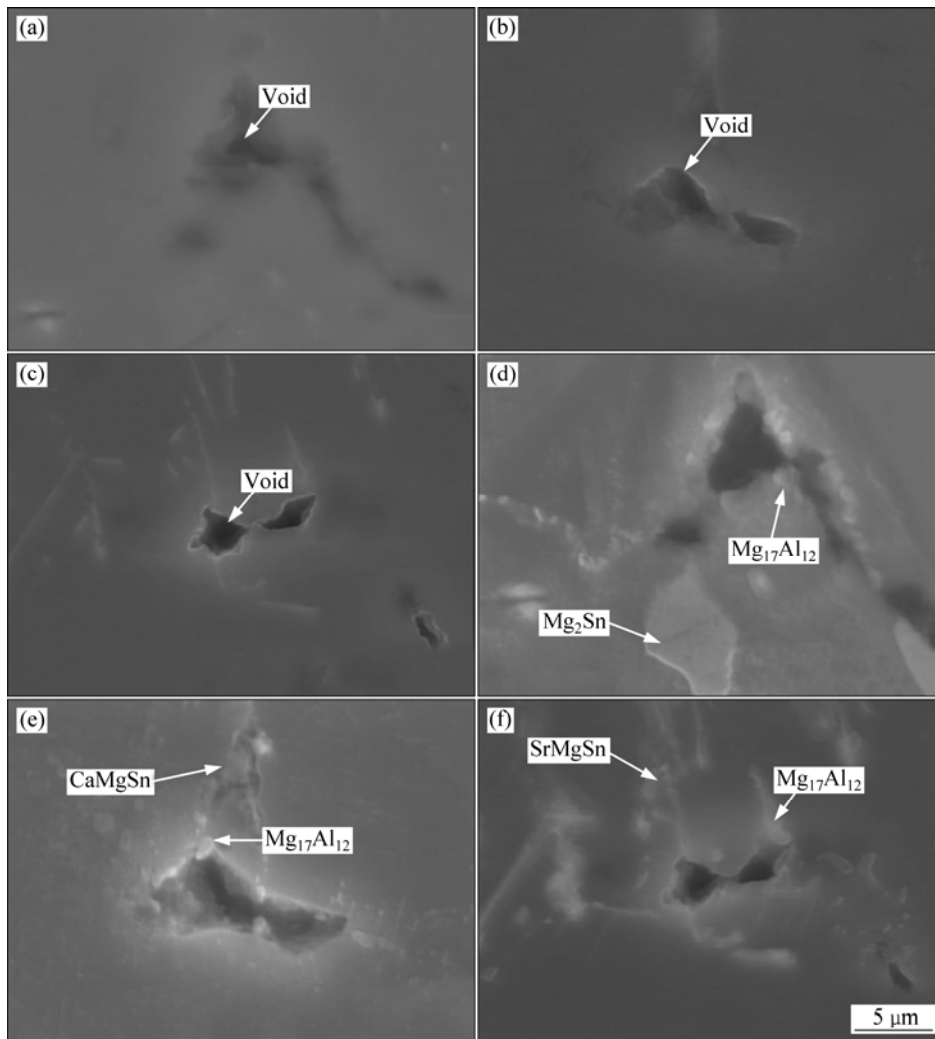


Fig.8 Void initiation of AT42 system alloys during creep test at 150 °C, 50 MPa: (a) Non-etched AT42; (b) Non-etched ATX421; (c) Non-etched ATJ421; (d) Etched AT42; (e) Etched ATX421; (f) Etched ATJ421

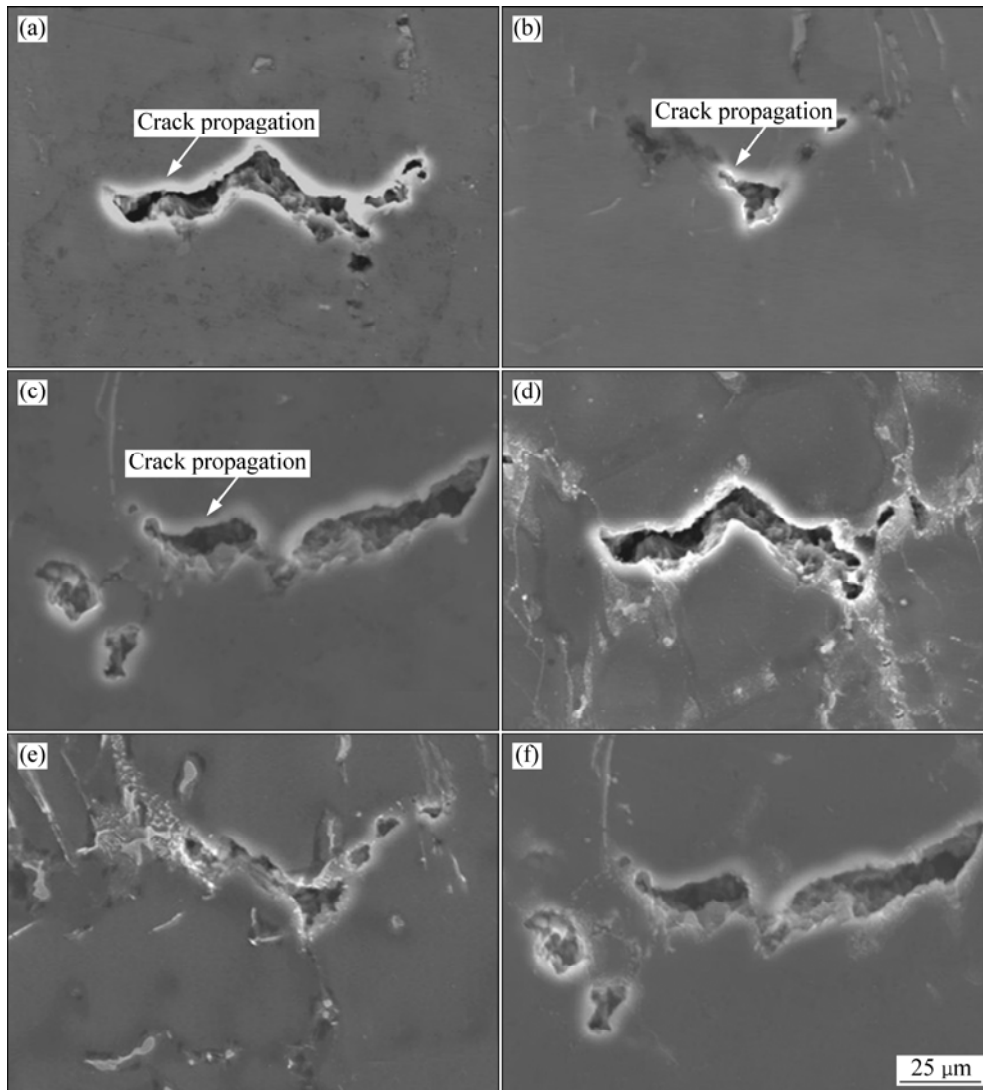


Fig.9 Crack propagation of AT42 system alloys after creep test at 150 °C, 80 MPa: (a) Non-etched AT42; (b) Non-etched ATX421; (c) Non-etched ATJ421; (d) Etched AT42; (e) Etched ATX421; (f) Etched ATJ421

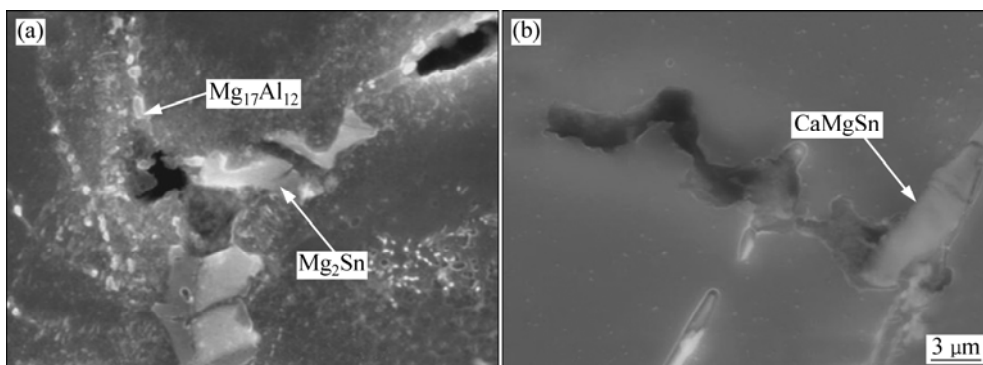


Fig.10 SEM images of creep specimens

However, in the creep tests, the voids were initiated mainly at the thermally unstable $Mg_{17}Al_{12}$ and the crack propagated along the grain boundaries. Moreover, the $CaMgSn$ and $SrMgSn$ phases were changed slightly,

which prevented crack propagation.

The deformation behavior suggests that the grain boundaries are the weakest link in these alloys because grain boundary cracking is evident without apparent

cracking within the grains. However, the thermally stable phases of SrMgSn and CaMgSn increase the grain boundary strength, and it is believed that the addition of Ca and Sr can improve the high temperature mechanical properties of the Mg alloy.

4 Conclusions

1) The Mg-4Al-2Sn alloy consisted of α -Mg, Mg₁₇Al₁₂ and Mg₂Sn phases. The addition of Ca and Sr resulted in the formation of CaMgSn and SrMgSn ternary phases within the grains.

2) The SrMgSn and CaMgSn ternary phases had an adverse effect on the room temperature tensile strength. However, the high temperature tensile strength was increased through the prevention of crack propagation.

3) Void initiation was observed at the Mg₁₇Al₁₂ phase, and cracks propagated along the grain boundaries. However, ternary phases of SrMgSn and CaMgSn effectively impeded the crack propagation.

Acknowledgments

This work was supported by a grant from the Metals Bank by the Ministry of Knowledge Economy and a grant-in-aid for the National Core Research Center Program (No. R15-2006-022-02001-0)

References

- [1] HENRY H, ALFRED Y, NAIYI L, ALLISON J E. Potential magnesium alloys for high temperature die cast automotive applications [J]. *Materials and Manufacturing Processes*, 2003, 18(5): 687–717.
- [2] MORDIKE B L, EBERT T. Magnesium [J]. *Materials Science and Engineering A*, 2001, 302: 37–45.
- [3] LUO A A, ANIL K S, RAJA K M. Magnesium extrusion development for automotive applications [C]// 64th Annual World Magnesium Conference Proceedings. Vancouver, Canada, 2007: 1–8.
- [4] PARK K C, KIM B H, HISAMICHI K, PARK Y H, PARK I M. Microstructure and corrosion properties of Mg-xSn-5Al-1Zn (x=0, 1, 5 and 9 mass%) alloys [J]. *Materials Transaction*, 2010, 51(3): 472–476.
- [5] KIM B H, LEE S W, PARK Y H, PARK I M. The microstructure, tensile properties, and creep behavior of AZ91, AS52 and TAS652 alloy [J]. *Journal of Alloys and Compounds*, 2010, 493: 502–506.
- [6] WANG J G, HSIUNG L M, NIEH T G, MABUCHI M. Creep of a heat treated Mg-4Y-3RE alloy [J]. *Materials Science and Engineering A*, 2001, 315: 81–88.
- [7] MENDIS C L, BETTLES C J, GIBSON M A, GROSSE S, HUTCHINSON C R. Refinement of precipitate distributions in an age-hardenable Mg-Sn alloy through microalloying [J]. *Philosophical Magazine Letters*, 2006, 86(7): 443–456.
- [8] SUZUKI A, SADDOCK N D, JONES J W, POLLOCK T M. Structure and transition of eutectic (Mg,Al)₂Ca Laves phase in a die-cast Mg-Al-Ca base alloy [J]. *Scripta Materialia*, 2004, 51: 1005–1010.
- [9] WAN Y, XIONG S, LIU W, ZOU Z. Effect of Si, Ca and Sr on the creep-resistance of AZ91D alloy [J]. *Materials Science Forum*, 2005, 488/489: 767–770.
- [10] LIHONG H, HENRY H, DEREK O. N. Effect of Ca additions on microstructure and microhardness of an as-cast Mg-5.0wt.%Al alloy [J]. *Materials Letters*, 2008, 62: 381–384.
- [11] SADDOCK N D, SUZUKI A, TERBUSH J R, JONES J W, POLLOCK T M. Creep Behavior of Permanent Mold Cast Mg-Al-Ca Based Alloys [C]// *Magnesium Technology 2007*. Florida, USA, 2007: 407–412.
- [12] JING B, YANGSHAN S, FENG X, SHAN X, JING Q, TIANBAI Z. Effect of Al contents on microstructures, tensile and creep properties of Mg-Al-Sr-Ca alloy [J]. *Journal of Alloys and Compounds*, 2007, 437: 247–253.
- [13] SPIGRELLI S, CERRI E, EVANGELISTA E, KLOC L, CADEK J. Interpretation of constant-load and constant-stress creep behavior [J]. *Materials Science and Engineering A*, 1998, 254: 90–98.
- [14] LUO A A. Recent magnesium alloy development for elevated temperature application [J]. *International Materials Reviews*, 2004, 49(1): 13–30.

(Edited by YANG Bing)